Model of Soft-Switching Converter and Power Control of Grid-Connected Photovoltaic Systems

Roberto Zanasi
DII-Information Engineering Department
University of Modena and Reggio Emilia,
Via Vignolese 905, 41100 Modena, Italy
Email: roberto.zanasi@unimore.it

Stefania Cuoghi
DII-Information Engineering Department
University of Modena and Reggio Emilia,
Via Vignolese 905, 41100 Modena, Italy
Email: stefania.cuoghi@unimore.it

***Abstract*—This paper presents a modeling technique, so called Power Oriented Graph, suitable for designing and simulating new topologies of inverter in energy generation system and reducing production cost. This technique is used for modeling a recently proposed soft-switching grid-connected DC/AC power converter for photovoltaic systems. Modifications in the structure of the DC/DC converter and in the control of the DC/AC converter are proposed. Simulation results confirm the effectiveness of the presented model and the introduced improvements.**

I. Introduction

In today's climate of growing energy needs and increasing environmental concern, the research interest on renewable energy, particularly on solar energy, is increasing. Over the last few years, electronic-based power conversion for distributed and renewable energy sources have evolved significantly. In particular, innovative inverter topologies have been suggested in the literature to provide many benefits and cost reduction. This is due to the important and critical role of the inverter and its control in the power conversion system of a photovoltaic (PV) structure. Many studies are still done to improve robustness, reliability, efficiency, size and weight of the inverters. In this scenario, modeling tools would be helpful to manufacturers to simulate new inverter topologies, reducing the time and the cost of design, see [1], [2]. In this paper an accurate model of a PV inverter architecture recently proposed in [3] is presented. The model has been obtained using the Power Oriented Graph (POG) technique [4]-[6]. The analyzed and simulated system is based on a single-phase 3kW DC/AC power converter, implementing an active-bridge DC/DC converter and a full-bridge DC/AC. The variant of an input half-bridge instead of an input full-bridge in the DC/DC converter is considered. Functional and mathematical analysis of the converter and the analytical form of the power flow are presented. The paper is organized as follows. In section II the system structure is presented. In section III the variant of the DC/DC converter is described, in section IV the POG modeling technique and the model of the PV inverter are presented. Simulations of the considered power conversion system and conclusions end the paper.

II. System structure

Let us consider the blocks scheme of the grid-connected PV system shown in Fig. 1, which is an improved version of

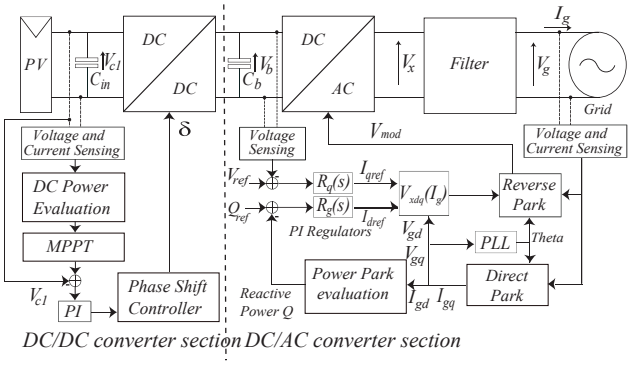

Fig. 1. Blocks scheme of the considered grid-connected PV system

the power converter proposed in [3]. The upper part represents the hardware section, which includes an active-bridge DC/DC converter, a single-phase buck 3kW DC/AC converter and a low-pass filter. The corresponding electrical circuit is shown in Fig. 2. In particular, the DC/DC converter is designed to boost the input voltage from a minimum input of 150V to a DC value regulated at 450 V. It is composed by an input full-bridge (FB) connected to an active half-bridge (HB) through an HF transformer, see sec. ②-⑤ in Fig. 2. This structure provides galvanic isolation between the PV array and the utility line, protecting the system against electric shocks and improving its safety. Moreover the transformer leakage inductance is used as energy storing and transferring element during the circuit operation. The DC/DC converter is controlled using the zero-voltage-switching (ZVS) PWM technique [7], [8] and operates in a soft-switched manner [9]. The DC/AC converter is composed by a IGBT full-bridge DC/AC converter PWM-controlled, see sec. ⑥-⑧ in Fig. 2. It is design to step down and to modulate the output voltage according to the grid voltage (230 Vrms $\pm 10\%$ and $49.7 - 50.3$ Hz). Finally the LCL low pass filter is used to reduce the high-frequency harmonics introduced by the PWM modulation on output voltage. The lower part of the blocks scheme in Fig. 1 represents the functional scheme of the converter control. In practical implementations the topology is controlled by a microprocessor, regulating the active and reactive powers flows, according to the European standards (EN 61727). In

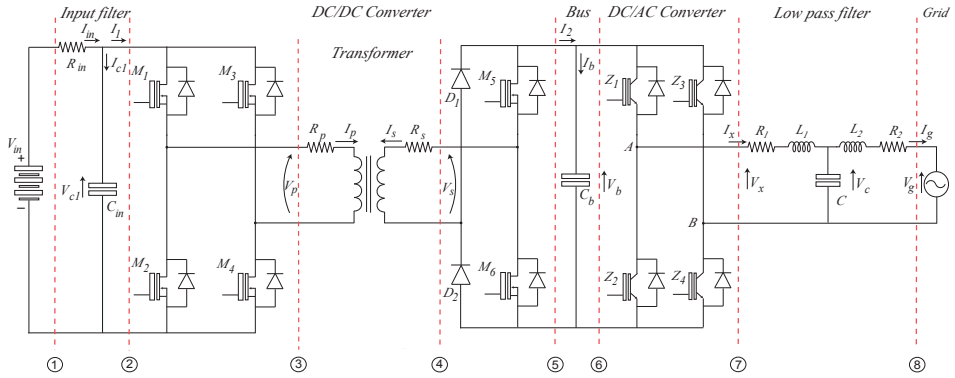

Fig. 2. Complete hardware structure of the PV system connected to the grid.

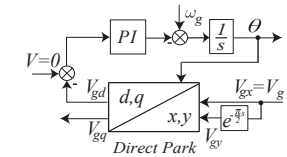

Fig. 3. Block diagram representation of PLL algorithm

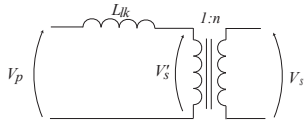

Fig. 4. Primary-referred equivalent circuit of the transformer.

particular, the DC/DC converter is controlled by regulating the phase-shift δ between the input bridge legs and the output bridge legs of the DC/DC converter. The control is based on a Maximum Power Point Tracking (MPPT) algorithm in order to extract the maximum possible power from the PV panels in all the irradiation conditions. In particular, the microprocessor implements an optimized version of the *perturb and observe method* described in [3] and [10]. The control of the DC/AC converter is designed to supply current into the utility line by regulating the bus voltage V_b to the constant value $V_{ref} = 450$V. The modulation voltage $V_{mod}(t)$ is regulated to synchronize the grid current $I_g(t)$ with the grid voltage $V_g(t)$, see Fig 2. The required synchronization is done by using a Phase Locked Loop (PLL) algorithm which detects the phase angle of the utility voltage, this is described in [3] and represented in Fig. 3. It is based on the Park transformations and Akagi's *pq* theory [11]-[14] to easily control error signals with constant reference values. The "Power Park evaluation" block shown in Fig. 1 calculates the reactive power Q flowing towards the grid, which is regulated to be equal to $Q_{ref} = 0$ by an indirect control of the reactive current flowing to the grid using Proportional and Integral (PI) compensators.

III. DC/DC CONVERTER SECTION

The operating principle of the converter is described in [3]. In this paper the variant of using an active half-bridge instead of active full-bridge is proposed. This solution has the advantage of decreasing the number of devices and the cost of the converter. Let us consider the primary-referred equivalent circuit of the transformer, see Fig. 4, where n is the transformer turn ratio, L_{lk} is the primary-referred leakage inductance and $V_s' = \frac{V_s}{n}$, see [8]. The main commutation waveforms during one switching cycle in steady state conditions are shown in Fig. 5, where $\theta = \omega t$, $\omega = 2\pi f_s$ and f_s is the switching frequency. Variable $M_i(\theta)$ denotes the control input of the i-th MOS: when $M_i = 1$ the MOS is ON, when $M_i = 0$ the MOS is OFF. The DC/DC converter is controlled by regulating the phase-shift δ between signal $M_5(\theta) = \overline{M}_6(\theta)$ of the active bridge and signal $M_1(\theta) = M_4(\theta)$ of the input bridge. The transformer secondary current I_s has the same behavior of primary current I_p with the opposite sign.

The converter operation modes are described below, see Fig. 5-8.

Before mode I. The initial conditions are as follows: $M_2 = M_3 = M_6 = 1$, $M_1 = M_4 = M_5 = 0$, $V_p = -V_{c1}$, $V_s = -V_b$, $I_p < 0$ and $I_s > 0$.

Mode I. For $0 < \theta < S_1$, the values of the control signals are $M_1 = M_2 = M_3 = M_4 = M_5 = 0$, $M_6 = 1$. The switching of M_2 and M_3 leads the primary current $I_p < 0$ to flow in diodes of MOS_1 and MOS_4, voltage V_p changes sign and current $I_s > 0$ flows in diodes of MOS_6 and D_1. For $S_1 < \theta < \Omega_1$, the values of the control signals are: $M_1 = M_4 = M_6 = 1$, $M_2 = M_3 = M_5 = 0$.

Mode II. Currents I_p and I_s change the flow direction and pass through MOS_1, MOS_4 and through MOS_6 and diode D_2 respectively. The values of the control signals are $M_1 = M_4 = M_6 = 1$ and $M_2 = M_3 = M_5 = 0$.

Mode III. The control signals switch to the values $M_1 = M_4 = M_5 = 1$ and $M_2 = M_3 = M_6 = 0$. The current I_p flows through MOS_1 and MOS_4, while I_s flows through diode D_2 and in the diode of MOS_5.

Mode IV. For $\pi < \theta < S_2$, it is $M_1 = M_2 = M_3 = M_4 = M_6 = 0$, $M_5 = 1$. Current $I_p > 0$ flows through diodes of MOS_3 and MOS_2, while $I_s < 0$ flows through diodes of MOS_5 and D_2. For $S_2 < \theta < \Omega_2$, it is $M_1 = M_4 = M_6 = 0$ and $M_2 = M_3 = M_5 = 1$.

Mode V. As in mode II, currents I_p and I_s change the flow direction. In this case the current $I_p < 0$ flows through MOS_3 and MOS_2, while $I_s > 0$ flows through MOS_5 and diode D_1.

Mode VI. In this case is $M_1 = M_4 = M_5 = 0$, $M_2 = M_3 = M_6 = 1$, the current $I_p < 0$ flows through MOS_3 and MOS_2 while $I_s > 0$ flows through the diode of MOS_6 and diode D_1.

The ranges $(0, S_1)$ and (π, S_2) in modes I and IV correspond to the dead-time periods. Since $S_1 << \delta'$, it can be assumed that $\delta \simeq \delta'$.

A. Mathematical model of the transformer

The dynamic behavior of the ideal transformer is described by the following equations

$$L_p \dot{I}_p + M \dot{I}_s = V_p - R_p I_p, \qquad L_s \dot{I}_s + M \dot{I}_p = V_s - R_s I_s, \quad (1)$$

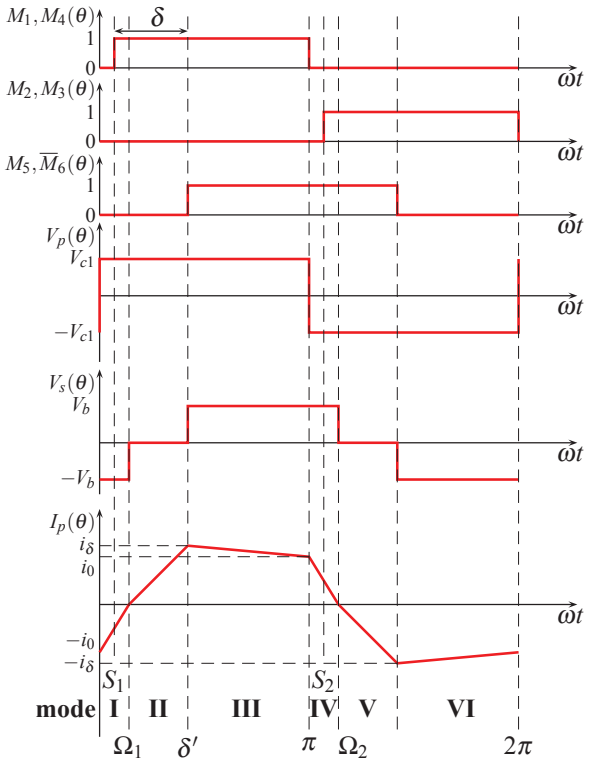

Fig. 5. Idealized voltage and current waveforms of the transformer.

where L_p, L_s and M are the self and mutual inductances of the transformer, R_p and R_s are the corresponding transformer resistances. Relations (1) can be expressed in the matrix form as follows

$$\begin{bmatrix} L_p & M \\ M & L_s \end{bmatrix} \begin{bmatrix} \dot{I}_p \\ \dot{I}_s \end{bmatrix} = \begin{bmatrix} -R_p & 0 \\ 0 & -R_s \end{bmatrix} \begin{bmatrix} I_p \\ I_s \end{bmatrix} + \begin{bmatrix} V_p \\ V_s \end{bmatrix}. \tag{2}$$

Applying the Laplace transformation to system (2) one obtains

$$\begin{bmatrix} I_p(s) \\ I_s(s) \end{bmatrix} = \begin{bmatrix} R_p + L_p s & Ms \\ Ms & R_s + L_s s \end{bmatrix}^{-1} \begin{bmatrix} V_p(s) \\ V_s(s) \end{bmatrix} = \frac{1}{\Delta(s)} \begin{bmatrix} R_s + L_s s & -Ms \\ -Ms & R_p + L_p s \end{bmatrix} \begin{bmatrix} V_p(s) \\ V_s(s) \end{bmatrix},$$

where $\Delta(s)$ is the determinant of the system

$$\Delta(s) = (L_p L_s - M^2)s^2 + (R_s L_p + R_p L_s)s + R_p R_s.$$

B. Mathematical expression for the power flow

From the converter operation modes previously described and from the idealized waveforms in steady-state conditions shown in Fig. 5, it follows that the Laplace transformed signals $V_p(s)$ and $V_s(s)$ can be expressed in a half switching period as follows

$$V_p(s) = \frac{V_{c1}}{s}\left(1 - 2e^{-\frac{\pi}{\omega}s}\right), \quad V_s(s) = \frac{V_b}{s}\left(-1 + e^{-\frac{\Omega_1}{\omega}s} + e^{-\frac{\delta}{\omega}s}\right).$$

Referring to the equivalent circuit of the transformer shown in Fig. 4, where $R_s = R_p = 0$ and due to symmetry during the two halves of the switching period, the primary current $I_p(\theta)$ can be expressed as follows

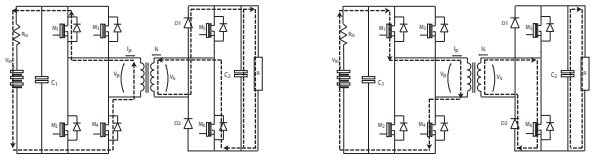

Fig. 6. Modes I and II

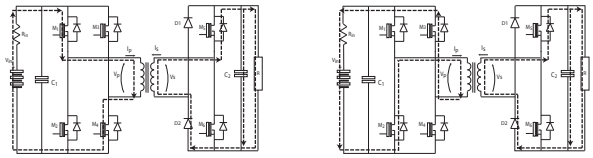

Fig. 7. Modes III and IV

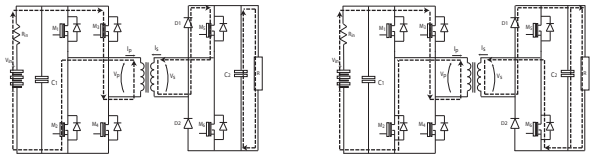

Fig. 8. Modes V and VI

$$\begin{aligned} I_p(\theta) &= -i_0 + \tfrac{V_{c1}(1+d)}{\omega L_{lk}}\theta && 0 \le \theta \le \Omega_1, \\ I_p(\theta) &= \tfrac{V_{c1}}{\omega L_{lk}}(\theta - \Omega_1) && \Omega_1 < \theta \le \delta, \\ I_p(\theta) &= i_\delta + \tfrac{V_{c1}(1-d)}{\omega L_{lk}}(\theta - \delta) && \delta < \theta \le \pi, \end{aligned} \tag{3}$$

where $d = \frac{V_b}{nV_{c1}}$. In (3) the phase shift δ between the input and the output bridges is assumed to be equal to δ', since $S_1 << \delta'$. The values of currents $i_0 = i_p(\pi) = -i_p(0)$ and $i_\delta = i_p(\delta)$ can be calculated using the first and the second relations of (3) for $\theta = \Omega_1$ and $\theta = \delta$,

$$i_0 = \frac{V_{c1}(1+d)}{\omega L_{lk}}\Omega_1, \qquad i_\delta = \frac{V_{c1}}{\omega L_{lk}}(\delta - \Omega_1). \tag{4}$$

Substituting (4) in the third equation of (3) for $\theta = \pi$, the following relation is obtained

$$\Omega_1 = \frac{\pi(1-d) + \delta d}{2+d}. \tag{5}$$

Assuming $0 < \Omega_1 < \delta$, the constraint $\delta > \pi\frac{d-1}{d}$ must be satisfied. The power P_{av} transferred to the output in a half switching period can be expressed as follows:

$$P_{av} = \frac{V_{c1}}{\pi}\left[\int_0^{\Omega_1} I_p(\theta)d\theta + \int_{\Omega_1}^{\delta} I_p(\theta)d\theta + \int_{\delta}^{\pi} I_p(\theta)d\theta\right]. \tag{6}$$

Substituting (3), (4) and (5) in (6) leads to the following expression of the power flow

$$\begin{aligned} P_{av} = \frac{V_{c1}^2 \pi d}{2\omega L_{lk}(2+d)^2}\Big[1 + d - 2d^2 + \\ + \left(\frac{\delta}{\pi}\right)4(d^2+d+1) - \left(\frac{\delta}{\pi}\right)^2 2(d^2+2d+2)\Big]. \end{aligned} \tag{7}$$

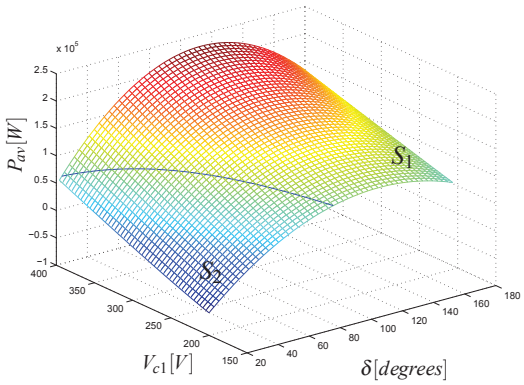

Fig. 9. Output power P_{av} of the DC/DC converter for $V_b = 450$V, $n = 1.5$ and $L_{lk} = 35\mu$H.

Assuming $V_b = 450$V and $n = 1.5$, it follows that $d \in (0.5, 1.9)$, see [3]. Given the value of L_{lk}, relation (7) shows how the output power P_{av} can be regulated choosing the values of parameters V_{c1} and δ. The plot of $P_{av}(\delta, V_{c1})$ is shown in Fig. 9, where only the surface S_1 satisfy the constraints $0 < \Omega_1 < \delta$ and $\delta > \pi\frac{d-1}{d}$.

IV. Power-Oriented Graphs Technique and Dynamic Model of the Hardware Structure

The Power-Oriented Graphs, see [4]-[6], is a graphical modeling technique suitable for modeling physical systems. The POG are normal block diagrams combined with a particular modular structure essentially based on the use of the two blocks shown in Fig. 10: the *elaboration block* stores and/or dissipates energy (i.e. springs, masses, dampers, capacities, inductances, resistances, etc.); the *connection block* redistributes the power within the system without storing or dissipating energy (i.e. any type of gear reduction, transformers, etc.). The main feature of the Power-Oriented Graphs is to keep a direct correspondence between the dashed sections of the graphs and real power sections of the modeled systems: the scalar product $\mathbf{x}^{\mathrm{T}}\mathbf{y}$ of the two *power vectors* $\mathbf{x}$ and $\mathbf{y}$ involved in each dashed line of a power-oriented graph, see Fig. 10, has the physical meaning of *the power flowing through that particular section*.

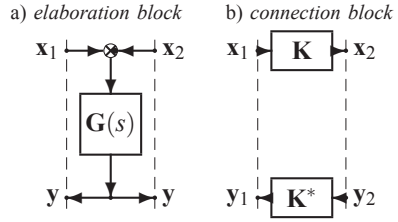

Fig. 10. POG: a) *elaboration block*; b) *connection block*.

The POG dynamic model of the electrical scheme given in Fig. 2 is shown in Fig. 11. The dashed lines ①-⑧ in Fig. 11 are in direct correspondence with the physical power sections ①-⑧ of Fig. 2: ①-② is the input filter; ②-⑤ is the DC/DC converter which includes the input bridge, the high frequency (HF) transformer and the output bridge; ⑤-⑦ includes the bus capacitor C_b and the DC/AC converter; ⑦-⑧ is LCL filter which connects the PV system to the grid. It is easy to see that the state space equations of the POG model of Fig. 11 can be expressed in the form $\mathbf{L}\dot{\mathbf{x}} = -\mathbf{A}\mathbf{x} + \mathbf{B}\mathbf{u}$ where:

$$\mathbf{L} = \begin{bmatrix} C_{in} & 0 & 0 & 0 & 0 & 0 \\ 0 & \mathbf{L}_T & 0 & 0 & 0 & 0 \\ 0 & 0 & C_b & 0 & 0 & 0 \\ 0 & 0 & 0 & L_1 & 0 & 0 \\ 0 & 0 & 0 & 0 & C & 0 \\ 0 & 0 & 0 & 0 & 0 & L_2 \end{bmatrix}, \quad \mathbf{x} = \begin{bmatrix} V_{c1} \\ \mathbf{I}_{ps} \\ V_b \\ I_x \\ V_c \\ I_g \end{bmatrix}, \quad \mathbf{I}_{ps} = \begin{bmatrix} I_p \\ I_s \end{bmatrix},$$

$$\mathbf{A} = \begin{bmatrix} \frac{1}{R_{in}} & \mathbf{K}_1^{\mathrm{T}} & 0 & 0 & 0 & 0 \\ -\mathbf{K}_1 & \mathbf{R}_T & -\mathbf{K}_2^{\mathrm{T}} & 0 & 0 & 0 \\ 0 & \mathbf{K}_2 & 0 & s_3 & 0 & 0 \\ 0 & 0 & -s_3 & R_1 & 1 & 0 \\ 0 & 0 & 0 & -1 & 0 & 1 \\ 0 & 0 & 0 & 0 & -1 & R_2 \end{bmatrix}, \quad \mathbf{B} = \begin{bmatrix} \frac{1}{R_{in}} & 0 \\ 0 & 0 \\ 0 & 0 \\ 0 & 0 \\ 0 & 0 \\ 0 & -1 \end{bmatrix},$$

$$\mathbf{u} = \begin{bmatrix} V_{in} \\ V_g \end{bmatrix}, \quad \mathbf{L}_T = \begin{bmatrix} L_p & M \\ M & L_s \end{bmatrix}, \quad \mathbf{R}_T = \begin{bmatrix} R_p & 0 \\ 0 & R_s \end{bmatrix}, \quad \mathbf{K}_1(s_1) = [s_1\ 0]^{\mathrm{T}} \quad \mathbf{K}_2(s_2) = [0\ s_2].$$

The dynamic model of the input bridge is described in Fig. 11 by the connection block ②-③ characterized by matrix $\mathbf{K}_1(s_1)$. The control signal $s_1(t)$ in time-domain is obtained as follows, neglecting the dissipative losses of the MOS:

$$s_1(t) = \frac{V_p(t)}{V_{c1}(t)} = \frac{I_1(t)}{I_p(t)} = 2\left(M_1(t) \oplus \overline{M}_3(t)\mathrm{sgn}\bar{I}_p(t) - 0.5\right),$$

where $V_{c1}(t)$ and $I_1(t)$ are respectively the DC/DC input voltage and current. Signal $s_1(\theta)$ has the same waveform of $V_p(\theta)$ in Fig. 5 normalized to values $\{1, -1\}$. The dynamic model of the output active bridge is described in Fig. 11 by means of the connection block ④-⑤ characterized by matrix $\mathbf{K}_2(s_2)$. The control signal $s_2(t)$ can be expressed as follows:

$$s_2(t) = \frac{V_s(t)}{V_b(t)} = \frac{I_2(t)}{I_s(t)} = \left(M_5(t)\bar{I}_s(t) - \overline{M}_5(t)I_s(t)\right),$$

where $V_b(t)$ and $I_2(t)$ are the output bus voltage and current. Signal $s_2(\theta)$ has the same waveform of $V_s(\theta)$ in Fig. 5 normalized to values $\{1, 0, -1\}$. The dynamic model of the transformer is described in section ③-④ by means of the matrices $\mathbf{L}_T$ e $\mathbf{R}_T$, see relation (2). Section ⑤-⑥ represents the model of the bus capacitor, while section ⑥-⑦ denotes the model of the IGBT full-bridge DC/AC converter. This converter is controlled by using a single-phase unipolar PWM modulation. The voltages of points A and B in Fig. 2 are separately regulated comparing the PWM triangular carrier $V_t(t)$ with the modulation voltage $V_{mod}(t)$ normalized with respect to the bus voltage $V_b(t)$. The control signal $s_3(t)$ can be expressed as follows:

$$s_3(t) = \frac{\mathrm{sgn}\left(V_t(t) + \frac{V_{mod}(t)}{V_b(t)}\right) - \mathrm{sgn}\left(V_t(t) - \frac{V_{mod}(t)}{V_b(t)}\right)}{2}, \qquad (8)$$

and the modulated voltage $V_x(t) = s_3(t)V_b(t)$ switches between the three levels $\{+V_b, -V_b, 0\}$. The POG model of the LCL

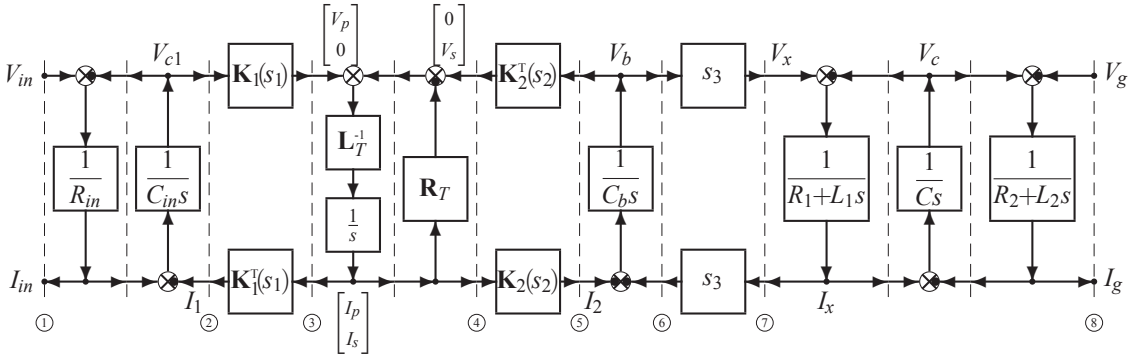

Fig. 11. POG dynamic model of the PV system described in Fig. 2.

filter is shown in section ⑦-⑧ of Fig. 11. The filter has been designed to reduce the high-order harmonics introduced by the PWM modulation, according to the methods described in [15] and [3].

A. Proposed control algorithm

The modulation voltage $V_{mod}(t)$ in (8) has to be chosen to synchronize the grid current $I_g(t)$ with the grid voltage $V_g(t)$ and to compensate the phase shift and the gain introduced by the filter at the grid frequency ω_g. Using the space vector representation, the modulation voltage can be expressed as $\overline{V}_{mod} = V_x(s)|_{s=j\omega_g}$. Taking into account the transfer function of the LCL filter, function $V_x(s)$ can be expressed as follows

$$V_x(s) = V_g(s)\,(1+R_1Cs+L_1Cs^2) + I_g(s)\,(L_1L_2Cs^3 + \\ +(L_1R_2+L_2R_1)Cs^2+(R_1R_2C+L_1+L_2)s+R_1+R_2).$$

Using the Park transformation, the modulation voltage V_x can be expressed in the transformed dq frame as follows

$$V_{xdq}(t) = \overline{V}_{gqd}(t)(1-L_1C\omega_g^2+jR_1C\omega_g)+ \\ +\overline{I}_{gref}(t)[R_1+R_2-(L_1R_2+L_2R_1)C\omega_g^2+ \\ +j((R_1R_2C+L_1+L_2)\omega_g-L_1L_2C\omega_g^3)], \qquad (9)$$

where $\overline{V}_{gdq}(t) = V_{gd}(t) + jV_{gq}(t)$ and $\overline{I}_{gref}(t) = I_{dref}(t) + jI_{qref}(t)$ are the complex vectors which describe the sensed grid voltage $V_g(t)$ and the desired grid current in the dq transformed frame, see Fig. 1. The reactive grid current $I_{dref}(t)$ is regulated by a PI compensator in order to have zero reactive power Q. The active grid current $I_{qref}(t)$ is dynamically controlled by a second PI compensator to maintain the bus voltage $V_b(t)$ equal to the desired value V_{ref}. Notice that the inner double PI structure used in [3] to generate the modulation voltage in the dq frame is substituted in the scheme of Fig. 1 by the block "$V_{xdq}(I_g)$" which implements relation (9).

V. Simulation Results

The presented simulation results have been obtained using the following parameters. DC/DC converter: $V_{in} = 300$ V, $R_{in} = 1\Omega$, $L_{lk} = 35\mu$H, $n = 1.5$, $L_p = 2.1$mH, $L_s = 4.8$mH, $M = 3.2$mH, $R_p = 0.15\Omega$, $R_s = 0.225\Omega$, DC/DC switching frequency $f_s = 35$kHz, $S_1 = 0.01\pi$ and $\delta = 0.234\pi$. DC/AC converter: PWM carrier frequency $f_c = 17\,kHz$, grid frequency $f_g = 50\,Hz$, $C = 5\,\mu F$, $L_1 = 1.8\,mH$, $L_2 = 0.9\,mH$, $R_1 = 0.1\,\Omega$, $R_2 = 0.05\,\Omega$ and $V_{ref} = 450$ V. PI controller $R_q(s)$ of variable I_{qref}: $R_q(s) = 1.8 + \frac{25}{s}$. PI controller $R_d(s)$ of variable I_{dref}: $R_d(s) = 0.001 + \frac{0.01}{s}$. PI controller $R_L(s)$ in the PLL algorithm: $R_L(s) = 1 + \frac{30}{s}$.

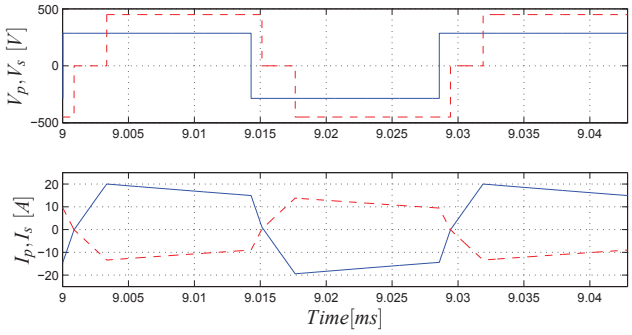

Fig. 12. Simulated primary and secondary currents and voltages.

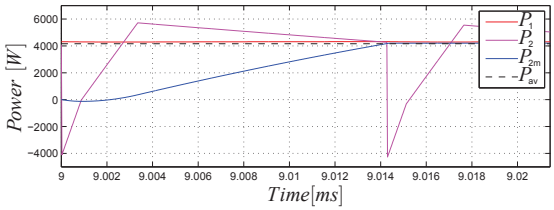

Fig. 13. Powers P_1 and P_2 flowing through sec. 1-2, total power P_{2m} flowing through sec. 2 in half switching period and theoretical output power P_{av}.

The waveforms of voltages and currents of the DC/DC converter are shown in Fig. 12, note that they exactly correspond to the idealized behaviors shown in Fig. 5. In steady state conditions the values of the input and bus voltages are $V_{c1} = 285.66 \pm 0.04$V and $V_b = 449.9 \pm 0.03$V. The values $i_0 = 14.95$A and $i_\delta = 19.99$A obtained in simulation well correspond to the values $i_0 = 15.2$A and $i_\delta = 19.7$A calculated using (4). The instantaneous powers $P_1 = V_{in}I_{in}$ and $P_2 = V_{c1}I_1$ flowing through sections ① and ② are shown in red and magenta lines in Fig. 13. The blue line denotes the total power $P_{2m} = \frac{V_{c1}}{\pi}\int_0^\pi i_p(\theta)d\theta$ flowing through sec. ② in a half switching period. Notice that the final value of P_{2m}, that is the mean power flowing in sec. ②, is equal to the theoretical output power P_{av} calculated using (7), see the black dashed

line, verifying the validity of (7). Moreover the value of P_{av} is equal to $P_1 - R_{in}I_{in}$ as expected.

The simulation results shown in Fig. 14-16 refer to the DC/AC section of the converter. The zoom in Fig. 14 shows signals V_g and I_g in steady-state condition. The proposed control algorithm (9) leads to a good synchronization of signals V_g and I_g. The powers P_5, P_6 and P_8 flowing through sections ⑤, ⑥, ⑧ of the system are shown in Fig. 15. In particular the blue line represents the power $P_5 = V_b I_2$ flowing through section ⑤, while the black and red lines represent the powers flowing through sections ⑥ and ⑧ of the POG scheme of Fig. 11. The ripple present on the power signals is mainly due to the current ripple and it depends on the *LCL* filter design [3]. The magenta and green lines shown in Fig. 15 represent, respectively, the active power P and the reactive power Q flowing towards the grid. In particular Fig. 15 shows that the mean value of the reactive power Q is equal to zero and the mean value of the active power P is nearly equal to power P_5. The system currents I_2, I_{gd}, I_{gq}, I_{dref} and I_{qref} obtained using an input sawtooth reference current I_2 are shown in Fig. 16, they perfectly correspond to the real waveforms obtained in practical implementation, see [3].

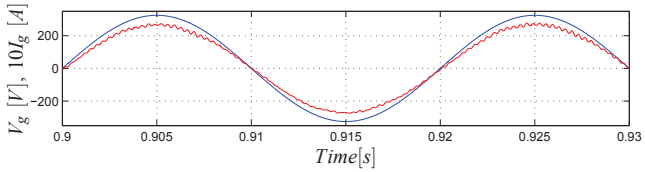

Fig. 14. Zoom of grid voltage Vg and grid current $10I_g$.

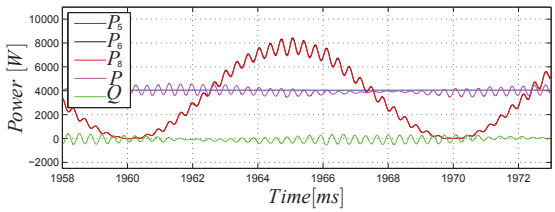

Fig. 15. Power flows P_5, P_6 and P_8 through sections 5, 6 and 8 of the POG scheme of Fig. 11. Active and reactive powers P and Q.

VI. Conclusion

In this paper a recent and innovative soft-switching converter for grid-connected PV systems has been considered. The mathematical model of the transformer and the mathematical expression of the output power of the DC/DC converter in the case of a input half-bridge have been described and introduced. In the paper the POG dynamic model and a new control strategy for the PV system connected to the grid have been presented. The main advantages of the proposed approach are the direct correspondence between POG sections and real power sections of the modeled system and the easy implementation of the POG graphs in Matlab-Simulink environment [4]. The presented simulation results confirm the validity of the POG model and the proposed control strategy. The utilized modeling technique seems to be useful to simulate new inverter topologies.

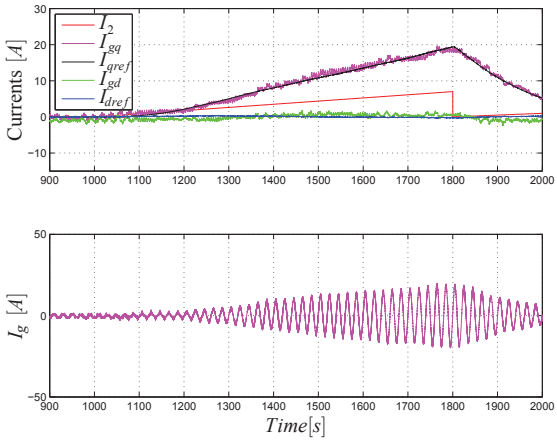

Fig. 16. Main currents in AD/DC section of the power converter when the input current I_2 is a sawtooth reference signal.

Acknowledgment

The authors would like to thank S. Culzoni, C. Tebaldi and M. Candeli.

References

[1] EIA, 2011, *Levelized cost of new generation resources in the Annual Energy Outlook* 2011. U.S. Energy Information Administration.

[2] K. Zweibel, *Should solar photovoltaics be deployed sooner because of long operating life at low, predictable cost?* Energy Policy, 38:7519-7530,2010.

[3] M. Cacciato, A. Casoli, R. Attanasio and F. Gennaro *Soft-switching converter with HF transformer for grid-connected photovoltaic systems*, IEEE Transactions on Industrial Electronics, 57(5):1678-86,2010.

[4] R. Zanasi, "Power Oriented Modelling of Dynamical System for Simulation", IMACS Symp. on Modelling and Control, Lille, France, May 1991.

[5] R. Zanasi, G. H. Geitner, A. Bouscayrol, W. Lhomme, "Different energetic techniques for modelling traction drives", ELECTRIMACS 2008, Qubec, Canada, June 8-11 2008.

[6] R. Zanasi, F. Grossi, "Modeling and Control of Power-Split Hybrid Electric Vehicles", Vehicular Power and Propulsion Conference VPPC 2010, Lille, France, 1-3 September 2010.

[7] Y. Jang, M. Jovanovic, Y. Chang, *A new ZVS-PWM full-bridge converter*. IEEE Trans. on Power Electron.: 18(5):1122-1129, Sept. 2003.

[8] H. Li, F. Peng, S. Lawler *A natural ZVS medium-power bidirectional DC-DC converter with minimum number of devices*. IEEE Trans. Ind. Applications.: 39(2), 525535, Mar./Apr. 2003.

[9] R.W. De Doncker, D.M. Divan, M.H. Kheraluwala, *A three-phase soft-switched high-power-density DC/DC converter for high-power applications*. IEEE Trans. on Industry Applications: 27(1):63-73, Jan/Feb 1991.

[10] D. Sera, R. Teodorescu, J. Hantschel, and M. Knoll, *Optimized maximum power point tracker for fast-changing environmental conditions*. IEEE Trans. Ind. Electron.: 55(7): 26262637, Jul. 2008.

[11] J.M. Kwon, K.H. Nam and B.H. Kwon. *Photovoltaic power conditioning system with line connection*. IEEE Trans.Ind.Electron.: 53(4):1048-1054, Jun. 2006.

[12] A. Yazdani and R. Iravani, *Voltage-Sourced Converters in Power Systems*. IEEE Pressed 2010.

[13] H. Akagi, Y. Kanagawae, and A. Nabae, *Instantaneous reactive power compensator comprising switching devices without energy storage components*. IEEE Trans. Ind. Appl.:IA-20(3), 625634, May/Jun. 1984.

[14] L. G. B. Rolim, D. R. da Costa, and M. Aredes, *Analysis and software implementation of a robust synchronizing PLL circuit based on the pq theory*. IEEE Trans. Ind. Electron.: 53(6), 19191926, Dec. 2006.

[15] M. Liserre, R. Teoderuscu, and F. Blaabjerg, *Stability of photovoltaic and wind turbine grid-connected inverters for a large set of grid impedance values*. IEEE Trans. Power Electron.: 21(1), 263272, Jan. 2006.